

Accepted Manuscript

Regulation of extracellular matrix degradation and metastatic spread by IQGAP1 through endothelin-1 receptor signaling in ovarian cancer

Lidia Chellini, Valentina Caprara, Francesca Spadaro, Rosanna Sestito, Anna Bagnato, Laura Rosanò



PII: S0945-053X(18)30303-2

DOI: <https://doi.org/10.1016/j.matbio.2018.10.005>

Reference: MATBIO 1535

To appear in: *Matrix Biology*

Received date: 13 July 2018

Revised date: 22 October 2018

Accepted date: 22 October 2018

Please cite this article as: Lidia Chellini, Valentina Caprara, Francesca Spadaro, Rosanna Sestito, Anna Bagnato, Laura Rosanò, Regulation of extracellular matrix degradation and metastatic spread by IQGAP1 through endothelin-1 receptor signaling in ovarian cancer. *Matbio* (2018), <https://doi.org/10.1016/j.matbio.2018.10.005>

This is a PDF file of an unedited manuscript that has been accepted for publication. As a service to our customers we are providing this early version of the manuscript. The manuscript will undergo copyediting, typesetting, and review of the resulting proof before it is published in its final form. Please note that during the production process errors may be discovered which could affect the content, and all legal disclaimers that apply to the journal pertain.

Regulation of extracellular matrix degradation and metastatic spread by IQGAP1 through endothelin-1 receptor signaling in ovarian cancer

Lidia Chellini¹, Valentina Caprara¹, Francesca Spadaro², Rosanna Sestito¹, Anna Bagnato¹, and Laura Rosanò^{1*}

¹Unit of Preclinical Models and New Therapeutic Agents, IRCCS - Regina Elena National Cancer Institute, Rome, Italy; ²Confocal Microscopy Unit, Core Facilities, Istituto Superiore di Sanità, Rome, Italy

Running title: β -arr1/IQGAP1 mediates signalling of ET-1 in invadopodia

Key words: invadopodia, endothelin-1, endothelin-1 receptors, ovarian cancer, β -arr1, IQGAP1

*Correspondence to: Dr. Laura Rosanò, Unit of Preclinical Models and New Therapeutic Agents, Translational Research Functional Departmental Area, Regina Elena National Cancer Institute, Via Elio Chianesi, 53, 00144 Rome, Italy. Phone: +39 06 52662590; e-mail: laura.rosano@ifp.gov.it.

Authors declare that there are not competing financial interests.

Abstract

The invasive phenotype of serous ovarian cancer (SOC) cells is linked to the formation of actin-based protrusions, invadopodia, operating extracellular matrix (ECM) degradation and metastatic spread. Growth factor receptors might cause engagement of integrin-related proteins, like the polarity protein IQ-domain GTPase-activating protein 1 (IQGAP1), to F-actin core needed for invadopodia functions. Here, we investigated whether IQGAP1 forms a “signalosome” with endothelin-1 (ET-1)/ β -arrestin1 (β -arr1) network, as signal-integrating module for adhesion components, cytoskeletal remodelling and ECM degradation. In SOC cells, ET-1 receptor (ET-1R) activation, besides altering IQGAP1 expression and localization, coordinates the binding of IQGAP1 with β -arr1, representing an “hotspot” for ET-1R-induced invasive signalling. We demonstrated that the molecular interaction of IQGAP1 with β -arr1 affects relocalization of focal adhesion components, as vinculin, and cytoskeleton dynamics, through the regulation of invadopodia-related pathways. In particular, ET-1R deactivates Rac1 thereby promoting RhoA/C activation for the correct functions of invasive structures. Silencing of either IQGAP1 or β -arr1, or blocking ET-1R activation with a dual antagonist, prevents matrix metalloproteinase (MMP) activity, invadopodial function, transendothelial migration and cell invasion. In vivo, targeting ET-1R/ β -arr1 signalling controls the process of SOC metastasis, associated with reduced levels of IQGAP1, as well as other invadopodia effectors, such as vinculin, phospho-cortactin and membrane type 1-MMP. High expression of ET_AR/ β -arr1/IQGAP1 positively correlates with poor prognosis, validating the clinical implication of this signature in early prognosis of SOC. These data establish the ET-1R-driven β -arr1/IQGAP1 interaction as a prerequisite for the dynamic integration of pathways in fostering invadopodia and metastatic process in human SOC.

Introduction

Among the different histological subtypes of ovarian cancer, ~90% include epithelial cancers and the most common diagnosed is serous ovarian cancer (SOC) [1]. Although in the last decade minimal improvement in mortality has been observed, 5-year overall survival is 25% for patients with stage III and stage IV cancer, highlighting the need to further explore molecular mechanisms underpinning invasive and metastatic behaviour and its relationship with the extent of disease [2]. Aggressive traits might be associated with the formation of invasive protrusions, invadopodia, characterized by the presence of a core of F-actin, associated with actin regulators (e.g., cortactin, cofilin), adaptor proteins (e.g., paxillin, TSK5), and matrix metalloproteases (MMP) (e.g., MMP-2, MMP-9, membrane type 1-MMP), which are surrounded by an adhesion ring containing adhesive components [3]. Invadopodia are activated in response to microenvironmental factors, such as extracellular matrix (ECM) stiffness or hypoxia, and growth factor receptor activation [4]. It has been previously demonstrated that integrins and adhesive components are essential to induce the formation of the invadopodial structures and that the dynamic changes of downstream signalling pathways are a prerequisite for a tight control of ECM degradation by invadopodia [5, 6]. In addition, the recruitment of proteinases and ECM degradation complete the maturation of invadopodia, in which integrin-associated proteins, like integrin-linked kinase (ILK), are engaged around the nascent actin structure, involving also IQ motif containing GTPase activating protein 1 (IQGAP1) [7-9]. IQGAP1 is overexpressed in a variety of cancers, including ovarian cancer and it binds multiple proteins, such as the small GTPases Cdc42, Rac1 and Rap1, facilitating their interactions [10-15]. IQGAP1 has multiple protein recognition-motifs to achieve its scaffolding function, offering the opportunity to compartmentalize and coordinate in a spatiotemporal manner different signalling proteins, playing a very central role in many cellular functions including migration and cytoskeletal architecture changes

[16]. In SOC, the endothelin-1 (ET-1) axis, including the peptide ligand ET-1 and two G-protein coupled receptors (GPCR) (ET_AR and ET_BR), is recognized as key regulator of tumor progression [17]. In SOC cells, autocrine activation of ET-1 receptors (ET-1R) is functionally involved in regulating cell-cell adhesion and communication, linked to epithelial to mesenchymal transition (EMT) and stem-cell like features, which dynamically regulate invasive and metastatic potential of these cells [17-19]. Concordantly, functional activation of ET_BR enhances protumorigenic activity both promoting the evasion of the immune response, and tumor angiogenesis/lymphangiogenesis [17]. One interesting feature of ET-1R activation is the dynamic recruitment of the protein β -arrestin (β -arr), serving as ligand-regulated adapter protein for selected intracellular proteins and the generation of cytosolic and nuclear “signalsomes” [20-27]. In particular, we identify β -arr1 as an integrator of ET-1-driven cytoskeleton and signalling network regulating invadopodia in SOC cells. Indeed, in response to ET-1, β -arr1 acts as a linker of different proteins, coupling RhoC GTPase activation, cytoskeleton architecture changes and formation/activation of invadopodia [28, 29].

Previous studies demonstrated that IQGAP1 is an important player in coordinating the balance between actin polymerization and MT1-MMP secretion in invadopodia, by linking adhesion with the exocytic delivery of MT1-MMP [9, 13]. Considering the interplay between IQGAP1 and upstream invadopodia signalling pathways, as Rho GTPases, focal adhesion components, and Arp2/3-N-WASP interacting complexes [30-33], in this study we delineate a network between β -arr1 and IQGAP1, as acto-adhesive and proteolytic signalling platform in ET-1R-driven invadopodia and ECM degradation in ovarian cancer.

Results

ET-1 upregulates IQGAP1 expression in SOC cells.

To study the potential involvement of IQGAP1 and β -arr1 interaction in ET-1R-driven invasive signalling, we analysed their expression in a panel of SOC cell lines, showing that IQGAP1 is expressed in 100% of these cells at both mRNA and protein levels (Fig. 1A, B), in parallel with β -arr1, and confirmed by immunofluorescence (IF) analysis (Fig. 1C). To test the possibility that ET-1 axis could affect the expression of IQGAP1 in these cells, we analysed its expression upon ET-1 stimulation. Fig. 1D and E show a two fold increase of IQGAP1 expression, at mRNA and protein levels, with a maximum after 24 hours of ET-1 addition, indicating that IQGAP1 expression is regulated by ET-1 in SOC cells.

ET-1R activation promotes interaction of IQGAP1 with β -arr1 to regulate Rho GTPases activity.

Based on previous findings showing that β -arr1 links different actin cytoskeleton regulators and that IQGAP1 participates in cytoskeleton remodelling and invadopodia function [14, 15, 22, 30-38], we hypothesized that ET-1R/ β -arr1 might regulate invasive potential by recruiting IQGAP1. As shown by co-IP assays, in both SKOV3 and HEY cells, ET-1 promotes the association of IQGAP1 with β -arr1, reaching a 2-4 fold increase after 60 min of stimulation (Fig. 2A and Supplementary Fig. 1A), which is inhibited by treatment with macitentan, a dual antagonist for ET_AR and ET_BR [39] (Fig. 2B). The interaction between IQGAP1 and β -arr1 is also confirmed by using cells exogenously expressed GFP-IQGAP1 and AU5- β -arr1 proteins upon ET-1 stimulation (Fig. 2C) or by GST-pull down assay, in which we observed a direct interaction between endogenous IQGAP1 and GST- β -arr1 fusion protein (Supplementary Fig. 1B). Moreover, confocal laser microscopy (CSLM) analysis and median co-localization value (Pearson's correlation) show cytosolic complexes of IQGAP1 with β -arr1 localized away from the plasma membrane in ET-1-

dependent manner, which are not observed after macitentan treatment (Fig. 3A). In addition, proximity ligation assays (PLA) between endogenous IQGAP1 and β -arr1 demonstrate that, in ET-1-dependent manner, these proteins interact each other and are in close proximity in both HEY and SKOV3 cells, establishing for the first time IQGAP1 as novel interactor of β -arr1 in ET-1-stimulated SOC cells (Fig. 3B and Supplementary Fig. 1C and D). Moreover, by performing PLA experiments and counterstaining with specific markers of Golgi (GM130) and early endosome (Rab5), we found that none of these markers were found to label the IQGAP1/ β -arr1 complexes (Supplementary Fig. 1C and D). On the other hand, we evaluated the effect of ET-1 on IQGAP1 localization in relation to F-actin. While plasma membrane localization of IQGAP1 is observed in control cells, ET-1 addition promotes the localization of IQGAP1 in areas of intense F-actin polymerization in dot-like structures, which is inhibited by macitentan treatment (Fig. 4), suggesting a putative involvement of IQGAP1 in the process of dynamic remodelling of cytoskeleton promoted by ET-1.

Then, we assessed the contribution of IQGAP1 as partner of β -arr1 in regulating dynamic activation of Rho GTPases. In SKOV3 and HEY cells, 2-fold-increase in RhoA activity and 2- and 3-fold increase in RhoC activity, respectively, is evident after ET-1 stimulation, which is inhibited by macitentan treatment, or either IQGAP1 or β -arr1 silencing (Fig. 5A and Supplementary Fig. 2A). Moreover, overexpression of IQGAP1-GFP promotes their activation, which is further potentiated by the addition of ET-1 (Supplementary Fig. 2B). Considering that IQGAP1 is known to constrain Rac1 activity to favour RhoA/RhoC activity [40-43], we examined the involvement of IQGAP1/ β -arr1 in regulating Rac1 activity. Addition of ET-1, in parallel to enhance RhoA/RhoC activation, decreases the activity of Rac1 of about 40%, while deletion of either IQGAP1 and β -arr1 restores its activity (Fig. 5B and Supplementary Fig. 3A,B), demonstrating that β -arr1/IQGAP1 complex is required for the fine regulation of ET-1-induced RhoA,C and Rac1 signalling in SOC cells. Previous

works reported RacGAP1 as a binding partner of IQGAP1 mediating Rac1 deactivation [44]. To test the possibility that RacGAP1 could act in our system as a complex with β -arr1 and IQGAP1, we performed IP experiments in HEY and SKOV3 cells and report a 3- and 2- fold enhanced association between RacGAP1, IQGAP1 and β -arr1 after ET-1 stimulus, respectively, which is impaired by macitentan treatment (Fig. 5C and Supplementary Fig. 3C). CSLM analysis shows that in ET-1-dependent manner RacGAP1 is recruited to β -arr1 (Supplementary Fig. 3D). Moreover, RacGAP1 silencing significantly impairs ET-1-dependent Rac1 deactivation and RhoA/C activity (Fig. 5D, E). These data demonstrate that ET-1 promotes the interaction of RacGAP1 with IQGAP1/ β -arr1, leading to suppression of Rac1 activity and activation of RhoA/C.

ET-1R axis regulates invadopodia activity through IQGAP1/ β -arr1 complex.

Since input from adhesion signalling is a critical regulatory event to invadopodia formation and IQGAP1 is an integrator of the cytoskeleton and cell adhesion machinery [6, 7], we evaluated the ET-1-driven IQGAP1 ability in affecting localization of the adhesion signalling components required for invadopodia formation process. As shown in Supplementary Fig. 4A, while in SCR-transfected cells vinculin localizes to filament-like structures at the tips of cells, which appeared to be focal adhesions, in ET-1-stimulated cells vinculin is mostly localized with F-actin in distinct punctate spots in the perinuclear ventral region of the cells, an effect which is absent upon silencing of IQGAP1. When considering the effects on the localization of a well-known invadopodia marker, such as TSK5 or cortactin, we found that compared to untreated cells, areas of cytosolic F-actin accumulation are enriched in vinculin, TSK5 or cortactin in cells upon ET-1 challenge, which is completely lost after macitentan treatment or IQGAP1 silencing (Supplementary Figure 4), indicating a potential involvement of IQGAP1 in the ET-1-induced invadopodia process. Considering the role of IQGAP1 in the invadopodia maturation process [9,13], we

analysed whether β -arr1/IQGAP1 might be a mediator of ET-1R-driven invadopodia function and ECM degradation. We examined the ability of cells to produce ventral actin protrusions when plated on fluorescent gelatin and assayed for matrix degradation in which the areas of degradations appear as spots in the matrix, with a loss of fluorescence. ET-1 stimulation significantly increases the ability of cells to degrade gelatin matrix and IQGAP1 localizes in the areas of F-actin dots and gelatin degradation, an effect that is lost after treatment concomitant with macitentan (Fig. 6 and Supplementary Fig. 5A and 6). Both IQGAP1 and β -arr1 silencing completely abolishes the localization of gelatin degradation with cortactin/vinculin signals (Fig.6 and Supplementary Fig. 5B and 6). Also, both IQGAP1 silencing and treatment with MMP inhibitor, Ilomastat, abolish the colocalization of F-actin/cortactin with degradation area (Supplementary Fig. 6), indicating that IQGAP1/ β -arr1 are players in the ET-1-driven invadopodia activity by coordinating adhesion and MMP activity at invadopodia structures.

IQGAP1/ β -arr1 network is required in the ET-1R-induced MMP activation and cell invasion.

Since enhanced secretion and activity of MMPs is a key feature of the ET-1-induced invasive phenotype of SOC cells [45], we performed gelatin zymography analyses. Macitentan treatment, or either IQGAP1 or β -arr1 silencing, negatively affects the ability of ET-1 to promote MMPs expression and secretion (Fig. 7A and Supplementary Fig. 5C). Then, we assessed the effect of ET-1-driven β -arr1/IQGAP1 network on SOC degradative and invasive capability in a 3D cell culture system using collagen matrix-embedded tumor spheroids derived from SOC cells, in which tumor cells are organized into a 3D structure mimicking a tumor micro-region or a micro-metastasis. In spheroid cultures from SKOV3 cells, ET-1 addition results in enhanced invasion into the surrounding matrix and radial outgrowth compared to control cells, which is impaired by silencing of IQGAP1 or β -arr1,

as well as by macitentan or I lomastat treatment (Fig 7B). In addition, 3D spheroid cells, transfected with a plasmid encoding GFP-IQGAP1, results in enhanced ability to invade in the surrounding matrix (Fig. 7B). By performing transwell chamber invasion assays, we confirmed the inhibitor effect of IQGAP1 silencing in ET-1-induced cell invasion, in both HEY and SKOV3 cells (Supplementary Fig. 7A). Moreover, the enhanced cell invasion due to IQGAP1 overexpression in SKOV3 cells is significantly reduced (50%) after treatment with the RhoA,B,C inhibitor (CT04), also upon ET-1 addition (Supplementary Fig. 7B), supporting the findings that the effect of IQGAP1 on cell invasion is linked to RhoA/C signalling. To determine the involvement of IQGAP1 in SOC cell extravasation from the blood vessel, we evaluated the ET-1-stimulated transendothelial migration through a monolayer of human umbilical endothelial cells (HUVEC). As shown in Fig. 7C, while in control cells, ET-1 enhances this capacity, both IQGAP1 and β -arr1 silencing strongly reduced this effect. Together, these results clearly suggest an association between stimulation of ET-1-driven β -arr1/IQGAP1 network as key node in the regulation of invasive behaviour and extravasation potential of SOC cells.

ET-1 receptor blockade impairs metastatic behaviour and interferes IQGAP1 expression.

To mimic aspects of SOC metastatic dissemination, we tested the effects of ET-1R blockade with macitentan in metastatic behaviour and molecular effectors of invadopodia by performing intraperitoneal (i.p.) injection. Mice in the control group show evident dissemination pattern of SKOV3 cells on the peritoneal surfaces, intestines, omentum, small bowel, liver, and spleen and ovaries. The average of i.p. nodules is significantly reduced in macitentan-treated mice, associated with a well-tolerated toxicity profile. Consistent with results obtained in vitro, in i.p. nodules from macitentan-treated mice, the inhibition of IQGAP1, vinculin, MT1-MMP expression, as well as phosphorylation of

cortactin is observed (Fig. 8B and C). These results indicate that the therapeutic efficacy of macitentan to control ET-1R/ β -arr1–driven SOC progression relies also on its ability to reduce critical regulators of invadopodia, such IQGAP1.

To determine the clinical relevance of mRNA expression of IQGAP1 alone and in combination with ET_AR (EDNRA) and β -arr1 (ARBB1), we investigated the prognostic significance in ovarian cancer patients using the KM plotter [47]. As shown in Fig. 8D and Supplementary Table 1-4, Kaplan-Meier analysis and the log-rank test demonstrate that high mRNA expression of IQGAP1 and combined IQGAP1/ARBB1 show a significant association with poor PFS among all ovarian cancer patients. The survival status of patients with EDNRA/ARBB1/IQGAP1 high expression is significantly worse than those of low expression group, as PFS [HR 1.52 (1.23-1.8), P=0.00011] (Fig. 8D), supporting the possibility that EDNRA/IQGAP1/ARBB1 could be used as prognostic biomarkers in SOC.

Discussion

We have identified a novel mechanism that coordinates invasive pathways downstream of ET-1R, in which the scaffolding protein IQGAP1 integrates signal output from this GPCR to invadopodia function in SOC cells by linking β -arr1 (Fig. 8E). This conclusion is based on the following major findings: 1. IQGAP1 interacts with β -arr1 in ET-1-stimulated SOC cells; 2. Engagement of IQGAP1 by β -arr1 favours the tight control of RhoA/C activity over Rac1, thereby coordinating invadopodia function and ECM degradation; 3. Interruption of ET-1R/IQGAP1/ β -arr1 network impairs invasive and metastatic behaviour; 4. Concomitant high expression of EDNRA/ARRB1/IQGAP1 is a negative prognostic factor in ovarian cancer patients.

Invadopodia are very dynamic membrane protrusions, whose function is to degrade components of ECM, enabling invasion and metastasis [3, 4, 46, 47]. To make a functionally active invadopodia, local concentration of ligands for mitogenic receptors, such as GPCR, acts as input for invadopodia assembly and maturation. Among well-recognized drivers of invadopodia, the ET-1R signalling is a crucial inducer, in which β -arr1 is instrumental for bringing and assembling cytoskeleton and signalling modules that direct the degradative activity at invadopodia [28, 29]. Indeed, ET-1R/ β -arr1 core is necessary to assemble elements for invadopodia formation, as cortactin and TSK5, as well as regulating invadopodia maturation [28, 29]. However, a deep understanding of how protein complexes, including effectors of invasive signalling, are assembled into a functional unit to enhance specific signalling pathways after ET-1R cue is not reached. Emerging data indicate that the interactions between scaffold proteins might determine the formation of unique signalosome to provide spatio-temporal organization of events in actin cytoskeleton signalling and function, and in this context IQGAP1 is considered a master signalosome for the plethora of IQGAP1-interacting proteins [15, 16].

According with previous data demonstrating the involvement of IQGAP1 in the progression and spread of ovarian cancer, and the role of IQGAP1 as potentially independent molecular predictor of highly aggressive tumors [12], our findings reveal a new mechanistic link between IQGAP1 and the progression of SOC, demonstrating that IQGAP1 is a new interactor of β -arr1 downstream of ET-1R signalling in shaping cytoskeleton remodelling, and invadopodia-dependent ECM degradation. It is conceivable that the interaction between IQGAP1 and β -arr1 might expand the potential of cross-talk between signalling cascades, highlighting an additional complexity in the molecular mechanism by which ET-1R regulates invadopodia. According with the role of IQGAP1 in delivering and accumulation of MT1-MMP at invadopodia dots [9,13], we propose that ET-1-dependent invadopodia maturation in SOC cells relies on the local coordination of effectors, such as RhoC and Rac1, triggered by the interaction of IQGAP1 with β -arr1. Since IQGAP1 possesses an inactive RasGAP domain lacking the ability to directly act as a GEF or GAP, we provide evidence that IQGAP1/ β -arr1 could act as small GTPase scaffolding platform, as RacGAP1, to promote GTP hydrolysis and consequently Rac1 inhibition and concomitant RhoA,C activation. Given that different inputs can promote selective Rho GTPase activation and inhibition, it is likely that ET-1R-guided β -arr1 interactions determine the convergence and activation/inhibition of specific signals for invadopodia, such as Rho GTPases, by recruiting GAP, as RacGAP1, where IQGAP1 helps to define the discrete locations and/or time. The coordination of cytoskeleton remodelling from ET-1R-driven IQGAP1/ β -arr1 interaction involves the organization and distribution of invasive components into an F-actin pool where other signalling converge for the generation of proteolytic protrusions, invasiveness, transendothelial migration and the metastatic spread of SOC cells. Considering also that IQGAP1 may participate in invadopodia formation as well as capture microtubules and microtubules motors for the formation and dynamics of

invadopodia [13], we can speculate that IQGAP1/ β -arr1 network might have additional functions in cytoskeleton changes occurring during invadopodia life-cycle.

The major fair of SOC patients is the propensity to recur as intraperitoneal metastatic disease, which occurs when tumor cells exfoliate from the primary tumor, permeate throughout the peritoneal cavity as single cells and multicellular aggregates, adhering to the mesothelial cells, and subsequently inducing submesothelial matrix invasion. In this context, SOC cells attach to the peritoneum and invadopodia mediate their invasion by degrading the ECM in the basement membrane, and stroma of the mesothelium [48].

Developing of new strategies to control metastatic disease before it emerges is an unmet need. Of note, targeting ET-1R activity by using the small molecule macitentan results in the impairment of ET-1R/ β -arr1-driven pathways and metastasis, correlating with reduced expression of IQGAP1 and other invadopodia effectors. These findings indicate that interfering with convergent ET-1R/ β -arr1 molecular complexes potentiating metastatic behaviour might represent a suitable anti-metastatic therapy for preventing invadopodia-mediated ECM and metastatic spread in human SOC.

In order to highlight new effective biomarkers for the early prognosis of SOC progression, we previously demonstrated that overexpression of ET_AR in SOC patients is associated with chemoresistance, EMT marker expression, and poor prognosis [18,19], indicating biological relevance of ET-1R as prognostic factor. The findings that high expression levels of EDNRA/ARRB1/IQGAP1 positively correlate with poor prognosis, further validate the clinical implication of these predictive markers in early prognosis of metastatic ovarian cancer patients.

Acknowledgments

We gratefully acknowledge Aldo Lupo for excellent technical assistance, Maria Vincenza Sarcone for secretarial assistance. This work was supported by Associazione Italiana Ricerca sul Cancro (AIRC) to L. R. (AIRC 12852), and A. B. (AIRC 14199).

Material and methods

Cell culture and treatments

Established human ovarian serous adenocarcinoma cell lines HEY, SKOV3 and CAOV3 were obtained from the American Type Culture Collection (LGC Standards, Teddington, UK). HEY cells were maintained in RPMI-1640 medium, SKOV3 cells were maintained in McCoy's 5A medium and CAOV3 cells were maintained in Dulbecco's modified Eagle Medium. All media was supplemented with 10% fetal calf serum, 50 units/ml penicillin and 50 mg/ml streptomycin. Cells were incubated at 37°C in a humidified atmosphere with 5% CO₂. When appropriate, cells were incubated in serum-free media with ET-1 (Sigma) at 100 nmol/l for the indicated times. Macitentan, also called ACT-064992 or *N*-(5-[4-bromophenyl]-6-{2-[5-bromopyrimidin-2-yloxy]ethoxy}pyrimidin-4-yl)-*N'*-propylsulfamide, was kindly provided by Actelion Pharmaceuticals Ltd (Allschwil, Switzerland) and was used at the concentration of 1 µmol/l for 30 min before the addition of ET-1. Ilomastat, also known as GM6001, (EMD Millipore, CA), a broad-spectrum matrix metalloproteinase inhibitor, is used at the concentration of 25 µM. Cell Permeable Rho Inhibitor (CT04) (Cytoskeleton, Inc.) is used at the concentration of 2 µg/mL.

Silencing and transient transfection

Cells were transfected using Lipofectamine 2000 (Thermo Fisher Scientific) according to the manufacturer's instructions. Cells were transfected for 48 hours and then lysed. Silencing of β -arr1 (L-011971-00), IQGAP1 (L-004694-00) and RacGAP1 (L-008650) was performed using ON-TARGET plus SMART pool siRNAs, or a negative control (D-001810-01) (Dharmacon). For ectopic expression of GFP-IQGAP1 and AU5- β -arr1, cells were transiently transfected with the plasmid pEGFP-IQGAP1 and the full-length β -arr1-AU5 plasmid, respectively. The plasmid pEGFP-IQGAP1 was a gift from David Sacks (Addgene plasmid #30112) and the full-length β -arr1-AU5 plasmid was kindly provided by Professor

Richard D Ye (Department of Pharmacology, College of Medicine, University of Illinois, Chicago, IL, USA).

Western Blotting (WB) and immunoprecipitation (IP)

For WB analysis, cells were lysed as previously described [29] and resolved on Mini-PROTEAN TGX gels (Biorad Laboratories). Immunoblotting was performed using the following primary antibodies (Abs): anti-IQGAP1 (cat no. ab86064, Abcam), anti- β -arr1 (cat no. ab32099, Abcam), anti-Tubulin (cat no. sc-32293, Santa Cruz Biotechnology), anti-HSP70 (cat no. ab2787, Abcam), anti-GFP (cat no. 83525, Immunological Science), anti-AU5 (cat no. ab24576, Abcam), anti-RacGAP1 (cat no. ab180802, Abcam), anti-MT1-MMP (cat no. 78738, Abcam), anti-cortactin (cat no. 3503, Cell Signalling), anti-phospho-cortactin Tyr 421 (cat no. 45696, Cell Signalling), anti-vinculin (cat no. sc-73614, Santa Cruz Biotechnology). Primary antibodies were revealed using horseradish peroxidase-conjugated goat anti-rabbit or anti-mouse Abs (Biorad Laboratories). For the immunoprecipitation (IP), precleared whole-cell lysates were incubated with anti-IQGAP1 (cat no. ab86064) and anti- β -arr1 (cat no. ab32099) Abs (Abcam) or the correspondent IgG control Ab (Thermo Fisher Scientific) and protein G agarose beads (Thermo Fisher Scientific) at 4°C overnight. For detection of co-immunoprecipitated β -arr1, HRP-conjugated protein A peroxidase (Thermo Fisher scientific) was used as secondary Ab. Proteins were visualized by chemiluminescence (Clarity Western ECL Substrates, Biorad Laboratories). Quantification analyses were performed by Chemi Doc Imaging System and Image Lab Software (Biorad Laboratories). For statistical analysis of immunoprecipitation experiments, co-immunoprecipitated protein band intensities were normalized to immunoprecipitated target protein, and band intensities were further normalized to unstimulated samples.

RNA isolation and RT-PCR

Total RNA was extracted from cells using Trizol Reagent (Thermo Fisher Scientific), according to the manufacturer's instructions and 1 µg were used for retrotranscription (RT) using Euro Script M-MLV Reverse Transcriptase (Euroclone). cDNA was examined by semiquantitative polymerase chain reaction (PCR), conducted in the automated DNA Thermal Cycler GeneAmp PCR System 9700 (Applied Biosystem) using AmpliTaq DNA Polymerase (Applied Biosystem). The primers used were as follow:

IQGAP1 F: 5'-ACCGTGGACCCAAAGAAC-3';

IQGAP1 R: 5'- CTTCCCGTAGAACTTTTTGTTG-3';

β-arr1 F: 5'-TCTCTGGGGCATACTGAACC-3';

β-arr1 R: 5'-GAGCACGCTTACCCTTTCAC-3';

CyclophilinA F: 5'-TTCATCTGCACTGCCAAGAC-3':

CyclophilinA R: 5'-TCGAGTTGTCCACAGTCAGC-3'.

The PCR products were analysed by electrophoresis on 1% agarose gel and visualized by using ChemiDoc Imaging System and ImageLab Software (Biorad Laboratories).

Immunofluorescence staining and Proximity Ligation Assay (PLA)

Cells cultured on coverslips were fixed with 4% paraformaldehyde, permeabilized with 0.2% Triton-X-100 and blockade with 0.1 M glycine, 1% BSA and 0.1% Tween20 in PBS. Abs against IQGAP1 (cat no. ab86064, Abcam), Cortactin (cat no. ab47768, Abcam), Vinculin (cat no. sc-73614, Santa Cruz Biotechnology), TKS5 (cat no.09-268, Millipore), RacGAP1 (cat no. ab180802, Abcam), β-arr1 (cat no. MAB2609, Millipore) were used followed by the appropriate anti-mouse and anti-rabbit Alexa-Fluor-488 and 594 secondary antibody (Thermo Fisher Scientific). Actin cytoskeleton was visualized using Alexa Fluor 488-phalloidin (Thermo Fisher Scientific). Nuclei were stained using 4',6'-diamidino-2-phenylindole (DAPI). Coverslips were mounted with Vectashield mounting medium for

fluorescence (Vector Laboratories Ltd, Peterborough, UK). All colocalization analyses were carried out using the Coloc2 plugin of ImageJ software to calculate Pearson's correlation coefficients. This software estimates the degree of overlap between fluorescence signals obtained in two separate fluorescent channels. The Pearson's coefficients were calculated from multiple images (n=15–45) from 3 independent experiments and then averaged and a standard deviation of the mean was calculated. Statistical analysis comparing Pearson's correlations amongst subtypes was completed with a one-way Anova with Tukey's multiple comparisons test.

For PLA experiments, after incubation with the primary Abs overnight at 4°C, cells were washed in PBS and then incubated with Duolink In Situ PLA Probe Anti-Mouse PLUS (DUO92001, Sigma-Aldrich, France) and Duolink In Situ PLA Probe Anti-Rabbit MINUS (DUO92005, Sigma-Aldrich, France) for 1 hr at 37°C. Then, coverslips were washed in PBS and then incubated with a DNA ligase diluted in Ligation buffer for 30 min at 37°C. After washing, coverslips were incubated with a DNA polymerase diluted in Amplification buffer for 120 min at 37°C. Fluorescence signals were captured by using a Leica DMIRE2 microscope equipped with a Leica DFC 350FX camera and elaborated by a Leica FW4000 deconvolution software (Leica). Anti-GM130 antibody (cat no. 610823, BD Transduction Laboratories) was used to visualize Golgi location and Cell Light Early Endosome-GFP (cat no. C10586, Life Technologies) was used to label early endosome.

Gelatin zymography

Conditioned media of untreated or treated cells were collected and analysed as previously reported [29].

Fluorescent gelatin degradation assay

Gelatin degradation assay was performed as described previously [29], using QCM Gelatin Invadopodia Assay (RED) (Millipore). The cells were incubated for 48 hrs in different experimental conditions and then processed for CLSM examinations, as previously described. Quantification of degraded gelatin area was performed using Cell Profiler software (www.cellprofiler.org).

Pull down assays

Rho GTP levels were assessed using a Rho-binding domain (RBD) affinity precipitation assay (Cytoskeleton, Inc.). To monitor Rac1 activation, Rac1 Activation Assay Biochem Kit (Cytoskeleton, Inc) was used according to the manufacturer's instructions. Cells were lysed in lysis buffer (50 mM Tris (pH7.5), 10mM MgCl₂, 0.5 M NaCl and 2% Igepal and proteases inhibitors) and 500 µg of cell extract was incubated with Glutathione S-transferase (GST)–Rhotekin coupled to glutathione agarose beads to pull down Rho A/C GTP form or PAK (p21-Activated protein Kinase)-PDB (p21 Binding Domain) beads to pull down Rac1-GTP form and samples were rotated at 4°C for 60 min. Beads were washed, and proteins were eluted in Laemmli Sample Buffer by heating to 95°C for 2 min. Proteins were analysed by WB and detection of Rho A/C GTP was performed by IB using anti-RhoA-B-C (cat no. 05-778, Millipore) or specific anti-RhoC (cat no.ab64659, Abcam) and anti-RhoA (cat no. ARH04, Cytoskeleton) Abs. Rac1-GTP was detected using anti-Rac1 Ab (cat no. ARC03, Cytoskeleton).

Recombinant protein purification and GST-pull down assay

The plasmid pGEX-4T1 β-arrestin1 [a gift from Robert Lefkowitz (Addgene plasmid #36918)] was transformed by heat shock into E. Coli BL21. Transformed cells were grown in LB medium, supplemented with 50 µg/ml Ampicillin, till an OD 600 of 0.6-0.7 and induced with 1 mM isopropyl-thiogalactoside (IPTG) for protein expression, at 25°C

overnight. From the cell-pellet, recombinant protein was purified using the MagneGST Protein Purification System (Promega), according to the manufacturer's instructions.

For GST-pull down assay, cell lysate was incubated with GST- β -arr1-beads for 3 hours at 4°C. After washes with PBS 1X, proteins were eluted in Leammi 2X by heating to 95°C for 5 min. Proteins were analysed by WB and detection of IQGAP1 or GST- β -arr1 was performed using IQGAP1 and GST (cat. no. SC-138 Santa Cruz) Abs.

3D-invasion assay

3D invasion assay was performed using Cultrex 3-D Spheroid Cell Invasion Assay (#3500-096-K) according to the manufacturer's instructions. SKOV3 cells spheroids were generated by plating 3000 cells for 48 hours in 3D Culture Qualified 96 Well Plate. Then, spheroids were embedded into invasion matrix. After 1 hour at 37°C, serum-free media with or without ET-1 and/or MAC and/or Ionomycin was added to spheroids wells. Plates were incubated for 72 hours and all spheroids were photographed using a phase-contrast microscope at X4 magnification. Quantification of invasion area and cumulative sprout length was performed using Image J Software.

Transendothelial migration assay

For the trans-endothelial migration, HUVEC were seeded (1×10^5 cells) in 8.0 μ m pore sized membranes BD BioCoat growth factor reduced Matrigel Invasion Chamber (BD Biosciences) and left to form a monolayer for 24 hrs at 37°C. Cells were analysed as previously described [29].

***In vivo* assay**

To mimic some aspects of SOC seeding on the peritoneal surfaces, representing typical metastatic sites observed in patients with an advanced stage of disease, female athymic (nu+/nu+) mice, 4–6 weeks of age (Charles River Laboratories, Milan, Italy) were injected

intraperitoneally (i.p.) with viable SKOV3 (2×10^6) cells following the guidelines for animal experimentation of the Italian Ministry of Health. Two weeks after, animals were randomized into two different groups of eight mice undergoing the following treatments for 5 weeks: (i) vehicle (CTR), (ii) macitentan (30mg/kg, oral daily). At the end of the treatment, all mice were euthanized and intraperitoneal organs were analysed. The number of visible intraperitoneal tumors was counted, removed, measured, carefully dissected, frozen and analysed by WB analysis. Values represent the mean \pm S.D. of eight mice for group from two independent experiments.

Kaplan-Meier analysis

The Kaplan–Meier plotter (<http://kmplot.com/analysis/>) [49] was used to investigate the correlation between combined expression of IQGAP1, ARRB1 and EDNRA mRNA levels (all probe sets for gene) and progression-free survival (PFS) starting from a cohort of 1435 ovarian cancer patients. These ovarian cancer patients derived from the Gene Expression Omnibus (GEO), the Cancer Biomedical Informatics Grid (caBIG), and The Cancer Genome Atlas (TCGA) datasets. The employed gene probes are as follow: 216235_s_at, 204464_s_at, 204463_s_at for EDNRA; 210840_s_at, 200791_s_at, 213446_s_at, 210790_s_at, 201542_at, 201543_s_at for IQGAP1; 228444_at, 218832_x_at, 222756_s_at, 222912_at for ARRB1. Ovarian cancer samples were divided into ‘low’ and ‘high’ according to gene mRNA expression using the auto select best cutoff value. Subsequently, PFS for the two groups were compared with a Kaplan–Meier survival plot on the webpage (<http://kmplot.com/analysis/index.php?p = service&cancer = ovar>). The ovarian cancer patients were followed up to 5 years. Hazard ratio (HR), 95% confidence intervals, and log rank P were presented on the main plots. P value of < 0.05 was considered to be statistically significant.

Statistical analysis

Statistical analyses were performed with the GraphPad Prism (GraphPad Software) and the values represent mean \pm SD obtained with not less than three independent experiments with similar results. The statistical significance of the differences was determined by the Student t-test for the comparisons between two groups; for more than two groups, the 1-way ANOVA analysis of variance was used.

For in vivo studies, a priori power analysis was performed using the G*Power statistical analysis program [50, 51]. By assuming two tails with normal distribution between two groups, calculations revealed that a sample size of $n=8$ would be sufficient to provide 95% power with 0.05 %-error probability and an effect size of 2.

References

- [1] R.L. Siegel, K.D. Miller, A. Jemal, Cancer Statistics, *Cancer J Clin* 67 (2017) 7-30.
- [2] A.N. Karnezis, K.R. Cho, C.B. Gilks, C.L. Pearce, D.G. Huntsman, The disparate origins of ovarian cancers: pathogenesis and prevention strategies, *Nat. Rev. Cancer* 17 (2017) 65-74.
- [3] E.K. Paterson, S.A. Courtneidge, Invadosomes are coming: new insights into function and disease relevance, *FEBS J.* 285 (2018) 8-27.
- [4] R.J. Eddy, M.D. Weidmann, V.P. Sharma, J.S. Condeelis, Tumor Cell Invadopodia: Invasive Protrusions that Orchestrate Metastasis, *Trends Cell Biol.* 27 (2017) 595-607.
- [5] E. Martín-Villar, B. Borda-d'Agua, P. Carrasco-Ramirez, J. Renart, M. Parsons, M. Quintanilla, G.E. Jones, Podoplanin mediates ECM degradation by squamous carcinoma cells through control of invadopodia stability, *Oncogene* 34 (2015) 4531-44.
- [6] O. Destaing, M.R. Block, E. Planus, C. Albiges-Rizo, Invadosome regulation by adhesion signalling, *Curr. Opin. Cell Biol.* 23 (2011) 597-606.
- [7] K.M. Branch, D. Hoshino, A.M. Weaver, Adhesion rings surround invadopodia and promote maturation, *Biol. Open.* 1 (2012) 711-22.
- [8] D. Rotoli, N.D. Pérez-Rodríguez, M. Morales, M.D. Maeso, J. Ávila, A. Mobasher, P. Martín-Vasallo, IQGAP1 in Podosomes/Invadosomes Is Involved in the Progression of Glioblastoma Multiforme Depending on the Tumor Status, *Int. J. Mol. Sci.* 18 (2017) pii: E150.
- [9] C. Petropoulos, C. Oddou, A. Emadali, E. Hiriart-Bryant, C. Boyault, E. Faurobert, S. Vande Pol, J. R. Kim-Kaneyama, A. Kraut, Y. Coute, M. Block, C. Albiges-Rizo, O. Destaing, Roles of paxillin family members in adhesion and ECM degradation coupling at invadosomes, *J. Cell Biol.* 213 (2016) 585-99.
- [10] M. Johnson, M. Sharma, B.R. Henderson, IQGAP1 regulation and roles in cancer, *Cell Signal.* 21 (2009) 1471-8.

- [11] L. Huang, S. Xu, D. Hu, W. Lu, X. Xie, X. Cheng, IQGAP1 Is Involved in Enhanced Aggressive Behavior of Epithelial Ovarian Cancer Stem Cell-Like Cells During Differentiation, *Int. J. Gynecol. Cancer* 25 (2015) 559-65.
- [12] P. Dong, K. Nabeshima, N. Nishimura, T. Kawakami, T. Hachisuga, T. Kawarabayashi, H. Iwasaki, Overexpression and diffuse expression pattern of IQGAP1 at invasion fronts are independent prognostic parameters in ovarian carcinomas, *Cancer Lett.* 243 (2006) 120-7.
- [13] M. Sakurai-Yageta, C. Recchi, G. Le Dez, J.B. Sibarita, L. Daviet, J. Camonis, C. D'Souza-Schorey, P. Chavrier, The interaction of IQGAP1 with the exocyst complex is required for tumor cell invasion downstream of Cdc42 and RhoA, *J. Cell Biol.* 181 (2008) 985-98.
- [14] S. Choi, R.A. Anderson, IQGAP1 is a phosphoinositide effector and kinase scaffold, *Adv. Biol. Regul.* 60 (2016) 29-35.
- [15] J.M. Smith, A.C. Hedman, D.B. Sacks, IQGAPs choreograph cellular signaling from the membrane to the nucleus, *Trends Cell Biol.* 25 (2015) 171-84.
- [16] T. Watanabe, S. Wang, K. Kaibuchi, IQGAPs as Key Regulators of Actin-cytoskeleton Dynamics, *Cell Struct. Funct.* 40 (2015) 69-77.
- [17] L. Rosanò, F. Spinella, A. Bagnato, Endothelin 1 in cancer: biological implications and therapeutic opportunities, *Nat. Rev. Cancer* 13 (2013) 637-51.
- [18] L. Rosanò, F. Spinella, V. Di Castro, M.R. Nicotra, S. Dedhar, A.G. de Herreros, P.G. Natali, A. Bagnato, Endothelin-1 promotes epithelial-to-mesenchymal transition in human ovarian cancer cells, *Cancer Res.* 65 (2005) 11649-57.
- [19] L. Rosanò, R. Cianfrocca, F. Spinella, V. Di Castro, M.R. Nicotra, A. Lucidi, G. Ferrandina, P.G. Natali, A. Bagnato, Acquisition of chemoresistance and EMT phenotype is linked with activation of the endothelin A receptor pathway in ovarian carcinoma cells, *Clin. Cancer Res.* 17 (2011) 2350-60.

- [20] L. Rosanò, A. Bagnato, β -arrestin1 at the cross-road of endothelin-1 signaling in cancer, *J. Exp. Clin. Cancer Res.* 35 (2016) 121.
- [21] Y.K. Peterson, L.M. Luttrell, The Diverse Roles of Arrestin Scaffolds in G Protein-Coupled Receptor Signaling, *Pharmacol. Rev.* 69 (2017) 256-297.
- [22] S. K. Shenoy, R. J. Lefkowitz, β -Arrestin-mediated receptor trafficking and signal transduction, *Trends Pharmacol. Sci.* 32 (2011) 521-33.
- [23] L. Rosanò, R. Cianfrocca, S. Masi, F. Spinella, V. Di Castro, A. Biroccio, E. Salvati, M.R., Nicotra, P.G. Natali, A. Bagnato, Beta-arrestin links endothelin A receptor to beta-catenin signaling to induce ovarian cancer cell invasion and metastasis, *Proc. Natl. Acad. Sci.* 106 (2009) N2806-11.
- [24] L. Rosanò, R. Cianfrocca, P. Tocci, F. Spinella, V. Di Castro, F. Spadaro, E. Salvati, A. M. Biroccio, P.G. Natali, A. Bagnato. β -arrestin-1 is a nuclear transcriptional regulator of endothelin-1-induced β -catenin signalling, *Oncogene* 32 (2013) 5066-77.
- [25] L. Rosanò, R. Cianfrocca, P. Tocci, F. Spinella, V. Di Castro, V. Caprara, E. Semprucci, G. Ferrandina, P.G. Natali, A. Bagnato, Endothelin A receptor/ β -arrestin signaling to the Wnt pathway renders ovarian cancer cells resistant to chemotherapy, *Cancer Res.* 74 (2014) 7453-64.
- [26] R. Cianfrocca, L. Rosanò, P. Tocci, R. Sestito, V. Caprara, V. Di Castro, R. De Maria, A. Bagnato, Blocking endothelin-1-receptor/ β -catenin circuit sensitizes to chemotherapy in colorectal cancer, *Cell Death Differ.* 10 (2017) 1811-1820.
- [27] R. Cianfrocca, P. Tocci, L. Rosanò, V. Caprara, R. Sestito, V. Di Castro, A. Bagnato, Nuclear β -arrestin1 is a critical cofactor of hypoxia-inducible factor-1 α signaling in endothelin-1-induced ovarian tumor progression, *Oncotarget* 14 (2016) 17790-804.

- [28] E. Semprucci, P. Tocci, R. Cianfrocca, R. Sestito, V. Caprara, M. Vegliione, V. Di Castro, F. Spadaro, G. Ferrandina, A. Bagnato, L. Rosanò, Endothelin A receptor drives invadopodia function and cell motility through the β -arrestin/PDZ-RhoGEF pathway in ovarian carcinoma, *Oncogene* 35 (2016) 3432-42.
- [29] F. Di Modugno, V. Caprara, L. Chellini, P. Tocci, F. Spadaro, G. Ferrandina, A. Sacconi, G. Blandino, P. Nisticò, A. Bagnato, L. Rosanò, hMEN1 is a key regulator in endothelin-1/ β -arrestin1-induced invadopodial function and metastatic process, *Proc. Natl. Acad. Sci.* 115 (2018) 3132-3137.
- [28] R. Cianfrocca, L. Rosanò, F. Spinella, V. Di Castro, P.G. Natali, A. Bagnato, β -arrestin-1 mediates the endothelin-1-induced activation of Akt and integrin-linked kinase, *Can. Physiol. Pharmacol.* 88 (2010) 796-801.
- [29] L. Rosanò, F. Spinella, V. Di Castro, S. Dedhar, M.R. Nicotra, P.G. Natali, A. Bagnato, Integrin-linked kinase functions as a downstream mediator of endothelin-1 to promote invasive behavior in ovarian carcinoma, *Mol. Cancer Ther.* 5 (2006) 833-42.
- [30] T. Watanabe, S. Wang, K. Kaibuchi, IQGAPs as Key Regulators of Actin-cytoskeleton Dynamics, *Cell Struct. Funct.* 40 (2015) 69-77.
- [31] A. Pelikan-Conchaudron, C. Le Clainche, D. Didry, M. F. Carlier, The IQGAP1 protein is a calmodulin-regulated barbed end capper of actin filaments: possible implications in its function in cell migration, *J. Biol. Chem.* 286 (2011) 35119-28.
- [32] L. B. Benseñor, H.M. Kan, N. Wang, H. Wallrabe, L.A. Davidson, Y. Cai, D.A. Schafer, G.S. Bloom, IQGAP1 regulates cell motility by linking growth factor signaling to actin assembly, *J. Cell Sci.* 120 (2007) 658-69.
- [33] C. Le Clainche, D. Schlaepfer, A. Ferrari, M. Klingauf, K. Grohmanova, A. Veligodskiy, D. Didry, D. Le, C. Egile, M. F. Carlier, R. Kroschewski, IQGAP1 stimulates actin assembly through the N-WASP-Arp2/3 pathway, *J. Biol. Chem.* 282 (2007) 426-35.

- [34] K.W. McGovern, K.A. DeFea, Molecular mechanisms underlying beta-arrestin-dependent chemotaxis and actin-cytoskeletal reorganization, *Handb. Exp. Pharmacol.* 219 (2014) 341-59.
- [35] M. Zoudilova, J. Min, H. L. Richards, D. Carter, T. Huang, K. A. DeFea, beta-Arrestins scaffold cofilin with chronophin to direct localized actin filament severing and membrane protrusions downstream of protease-activated receptor-2, *J. Biol. Chem.* 285 (2010) 14318-29.
- [36] T.T. Li, M. Alemayehu, A. Aziziyeh, C. Pape, M. Pampillo, L.M. Postovit, G.B. Mills, A.V. Babwah, M. Bhattacharya, Beta-arrestin/Ral signaling regulates lysophosphatidic acid-mediated migration and invasion of human breast tumor cells, *Mol. Cancer Res.* 7 (2009) 1064-77.
- [37] M. Alemayehu, M. Dragan, C. Pape, I. Siddiqui, D. Sacks, G.M. Di Guglielmo, A. V. Babwah, M. Bhattacharya, β -Arrestin2 regulates lysophosphatidic acid-induced human breast tumor cell migration and invasion via Rap1 and IQGAP1, *PLoS One* 8 (2013) e56174.
- [38] A. Javadi, R. K. Deevi, E. Evergren, E. Blondel-Tepaz, G.S. Baillie, M. G. Scott, F.C. Campbell, PTEN controls glandular morphogenesis through a juxtamembrane β -Arrestin1/ARHGAP21 scaffolding complex, *Elife* 6 (2017) pii: e24578.
- [39] M. Iglarz, C. Binkert, K. Morrison, W. Fischli, J. Gatfield, A. Treiber, T. Weller, M.H. Bolli, C. Boss, S. Buchmann, B. Capeleto, P. Hess, C. Qiu, M. Clozel, Pharmacology of macitentan, an orally active tissue-targeting dual endothelin receptor antagonist, *J. Pharmacol. Exp. Ther.* 327 (2008) 736-45.
- [40] G. Jacquemet, M.R. Morgan, A. Byron, J.D. Humphries, C.K. Choi, C.S. Chen, P.T. Caswell, M.J. Humphries, Rac1 is deactivated at integrin activation sites through an IQGAP1-filamin-A-RacGAP1 pathway, *J. Cell Sci.* 126 (2013) 4121-35.

- [41] D. E. Casteel, S. Turner, R. Schwappacher, H. Rangaswami, J. Su-Yuo, S. Zhuang, G. R. Boss, R. B. Pilz, Rho isoform-specific interaction with IQGAP1 promotes breast cancer cell proliferation and migration, *J. Biol. Chem.* 287 (2012) 38367-78.
- [42] Y. Wu, Y. Tao, Y. Chen, W. Xu, RhoC regulates the proliferation of gastric cancer cells through interaction with IQGAP1, *PLoS One* 7 (2012) e48917.
- [43] Y. Wu, Y. C. Chen, J. R. Sang, W. R. Xu, RhoC protein stimulates migration of gastric cancer cells through interaction with scaffold protein IQGAP1, *Mol. Med. Rep.* 4 (2011) 697-703.
- [44] G. Jacquemet, D.M. Green, R.E. Bridgewater, A. von Kriegsheim, M.J. Humphries, J.C. Norman, P.T. Caswell, RCP-driven $\alpha 5\beta 1$ recycling suppresses Rac and promotes RhoA activity via the RacGAP1-IQGAP1 complex, *J. Cell Biol.* 202 (2013) 917-35.
- [45] L. Rosanò, M. Varmi, D. Salani, V. Di Castro, F. Spinella, P.G. Natali, A. Bagnato, Endothelin-1 induces tumor proteinase activation and invasiveness of ovarian carcinoma cells, *Cancer Res.* 61 (2001) 8340-6.
- [46] S. Mrkonjic, O. Destaing, C. Albiges-Rizo, Mechanotransduction pulls the strings of matrix degradation at invadosome, *Matrix Biol.* 57-58 (2017) 190-203.
- [47] T.T. Chang, D. Thakar, V.M. Weaver, Force-dependent breaching of the basement membrane, *Matrix Biol.* 57-58 (2017) 178-189.
- [48] T. L. Yeung, C.S. Leung, K.P. Yip, C.L. Au Yeung, S.T.C. Wong, S.C. Mok, Cellular and molecular processes in ovarian cancer metastasis. A Review in the Theme: Cell and Molecular Processes in Cancer Metastasis. *Am. J. Physiol. Cell Physiol.* 7 (2015) C444-C456.
- [49] B. Gyorffy, A. Lánckzy, Z. Szállási, Implementing an online tool for genome-wide validation of survival-associated biomarkers in ovarian-cancer using microarray data from 1287 patients, *Endocr. Relat. Cancer* 19 (2012) 197-208.

[50] F. Faul, E. Erdfelder, A. Buchner, A. G. Lang, Statistical power analyses using G*Power 3.1: tests for correlation and regression analyses, *Behav. Res. Methods* 41 (2009) 1149–1160.

[51] J. Charan, N.D. Kantharia, How to calculate sample size in animal studies? *J. Pharmacol. Pharmacother.* 4 (2013) 303–306.

Figure legend

Figure 1. ET-1 regulates IQGAP1 in SOC cells. (A) Representative RT-PCR analysis showing endogenous IQGAP1 and β -arr1 mRNA levels in indicated cell lines. CyclophilinA (CypA) was used as loading control. **(B)** Representative Western blot (WB) analysis of endogenous IQGAP1 and β -arr1 expression in indicated cell lines. Tubulin was used for normalization. **(C)** Representative images of immunofluorescence analysis of IQGAP1 expression (green) in indicated cells. Nuclei were stained with DAPI (40,6-diamidino-2-phenylindole) (blue). Scale bar, 50 μ m. **(D)** Representative RT-PCR analysis for IQGAP1 mRNA in HEY cells stimulated with ET-1 (100nM) for the indicated times. CypA was used for normalization and quantification. **(E)** Lysates of HEY cells stimulated with ET-1 for the indicated times were analyzed for IQGAP1 expression. Tubulin was used for normalization and quantification. In (D) and (E), data represent the mean \pm SD from three independent experiments. Statistics were obtained using the one-way ANOVA test.

Figure 2. IQGAP1 is a new interactor of β -arr1 downstream of ET-1 signalling. (A) Lysates of SKOV3 cells incubated with ET-1 (100 nM) for the indicated times were immunoprecipitated with anti- β -arr1 Ab or control IgG. Immunoprecipitates (IP) and inputs were subjected to WB for IQGAP1 or β -arr1 expression. **(B)** Lysates of HEY cells incubated with ET-1 and/or MAC (1 μ M) for 60 min were immunoprecipitated with anti-IQGAP1, anti- β -arr1 Ab or control IgG. IP and inputs were subjected to WB for IQGAP1 or β -arr1 expression. In (A) and (B), data represent the mean \pm SD from three independent experiments of the average band intensity of IQGAP1 in β -arr1 IP normalized to unstimulated cells (Ctr) and shown as fold of Ctr. Statistics were obtained using the one-way ANOVA test. **(C)** Lysates of HEY cells, transfected with IQGAP1-GFP and β -arr1-AU5 and cultured with/without ET-1 for 60 min, were immunoprecipitated with anti-AU5 Ab. IP and inputs were subjected to WB for IQGAP1-GFP or β -arr1-AU5 expression. Data

represent the mean \pm SD from three independent experiments of the average band intensity of GFP-IQGAP1 in AU5- β -arr1 IP normalized to unstimulated cells (Ctr) and shown as fold of Ctr. Statistics were obtained using the Student's t-test.

Figure 3. IQGAP1 links β -arr1 in ET-1R-dependent manner. (A) Confocal laser scanner microscopy (CLSM) examination in HEY cells stimulated with ET-1 and/or MAC for 60 min and stained for IQGAP1 (green) or β -arr1 (red). Nuclei are reported in blue (DAPI). Scale bar= 30 μ m. Histograms, the mean \pm SD of Pearson's correlation (>50 cells for at least 3 independent experiments). Statistic was obtained using the one-way ANOVA test. **(B)** Representative image of proximity ligation assay (PLA) detection of IQGAP1 and β -arr1 complexes in HEY cells stimulated with ET-1 and/or MAC for 60 min. Red signal represents positive PLA reaction, and DAPI staining (blue) highlights the nucleus. Scale bar, 50 μ m. The quantification of the number of PLA dots per nucleus is presented with the mean \pm SD from the quantification of signals observed in about 50 cells chosen randomly in 5 different fields from 3 independent experiments. Statistics were obtained using the one-way ANOVA test.

Figure 4. ET-1 promotes relocation of IQGAP1 to F-actin. CLSM examination in SKOV3 cells stimulated with ET-1 and MAC for 60 min, and stained for IQGAP1 (green) or phalloidin (to detect F-actin; red). Nuclei are reported in blue (DAPI). IQGAP1/F-actin colocalization (white arrows). Scale bar= 30 μ m. Histograms, the mean \pm SD of Pearson's correlation (>30 cells for at least 3 independent experiments). Statistic was obtained using the one-way ANOVA test.

Figure 5. ET-1-driven IQGAP1/ β -arr1 interaction mediates Rho GTPase activities through RacGAP1. (A) Rhotekin beads were used to pull down RhoA and C-GTP from si-

SCR, si-IQGAP1 and si- β -arr1 transfected SKOV3 cells stimulated with ET-1 and/or MAC for 5 min. Pull down samples and inputs were analysed by WB for the indicated proteins. Histograms, the mean \pm SD from three different experiments of densitometric measurements of RhoA and C activity normalized to RhoA,B,C expression and shown as fold over si-SCR; statistics were obtained using the one-way ANOVA test. **(B)** GST-Pak1-PBD beads were used to pull down Rac1-GTP from si-SCR, si-IQGAP1 and si- β -arr1 transfected HEY cells stimulated with ET-1 and/or MAC for 5 min. Pull down samples and inputs were analysed by WB for the indicated proteins. Histograms, the mean \pm SD from three different experiments of densitometric measurements of Rac1 activity normalized to Rac1 expression and shown as fold over si-SCR; statistics were obtained using the one-way ANOVA test. **(C)** Lysates of HEY cells stimulated for 5 min with ET-1 were immunoprecipitated with anti- β -arr1 Ab. IP and inputs were subjected to WB for indicated proteins. Histograms, the mean \pm SD from three independent experiments of the average band intensity of IQGAP1 or RacGAP1 in β -arr1 IP normalized to unstimulated cells (Ctr) and shown as fold of Ctr. Statistics were obtained using the one-way ANOVA test. **(D)** GST-Pak1-PBD beads were used to pull down Rac1-GTP from si-SCR or si-RacGAP1 transfected HEY cells stimulated with ET-1 for 5 min. Pull down samples and inputs were analysed by WB for the indicated proteins. Histograms, the mean \pm SD of from three different experiments densitometric measurements of Rac1 activity normalized to Rac1 expression and shown as fold over si-SCR; statistics were obtained using the one-way ANOVA test. **(E)** Rhotekin beads were used to pull down RhoA and C-GTP from si-SCR, si-RacGAP1 transfected HEY cells stimulated with ET-1 for 5 min. Pull down samples and inputs were analysed by WB for the indicated proteins. Histograms, the mean \pm SD from three different experiments of densitometric measurements of RhoA and C activity normalized to RhoA,B,C expression and shown as fold over si-SCR; statistics were obtained using the one-way ANOVA test.

Figure 6. IQGAP1/ β -arr1 participates to invadopodia activity in ET-1R-dependent manner. CSLM analysis of HEY cells, transfected with si-SCR or si-IQGAP1 or si- β -arr1, plated onto gelatin and treated with ET-1 for 48 hrs. Representative images show gelatin (red), cortactin (green), vinculin (violet) and DAPI (blue). Scale bar= 30 μ m. Orthogonal views (y-z plane; x-z plane) indicate (arrows) areas of gelatin degradation where vinculin/cortactin co-localize. Histograms, the mean \pm SD of normalized degradation area (% of cells) from three independent experiments. Statistics were obtained using the one-way ANOVA test.

Figure 7. IQGAP1/ β -arr1 regulates ET-1-driven MMP activation, transendothelial migration and cell invasion. (A) Representative images of conditioned media from HEY cells transfected with si-SCR, si-IQGAP1 or si- β -arr1, treated with ET-1 and/or MAC for 48 hrs and analyzed by gelatin zymography. Arrows denote active forms of MMP-9 and MMP-2. Media were analyzed by WB and BSA signal was visualized using Ponceau staining. Histograms, the mean \pm SD from three different experiments of levels of the gelatinase activity quantified by densitometry, and normalized to BSA signals. Statistics were obtained using the one-way ANOVA test. **(B)** Representative images of 3D spheroid invasion assays over 6 days following the addition of invasion matrix, using si-SCR, si-IQGAP1, si- β -arr1 or IQGAP1-GFP expressing plasmid transfected SKOV3 cells, treated with ET-1 (100 nM) and/or MAC (1 μ M) and/or Ilomastat (25 μ M), and/or the Rho Inhibitor CT04 (2 μ g/ml). Histograms, quantification of 3D invasion relative to cumulative sprout length and invasion area, represent mean \pm SD from three different experiments; statistics were obtained using the one-way ANOVA test. Scale bar=100 μ m. **(C)** Fluorescence labelled si-SCR, si-IQGAP1 or si- β -arr1 transfected HEY cells applied onto the upper chamber with a monolayer of HUVEC on a cultrex-coated membrane. After 16 hrs, cells migrated through

the endothelial layer and membrane pores were photographed. Histograms, mean \pm SD from the quantification of signals in 15 different fields from 3 independent experiments from three different experiments; statistics were obtained using the one-way ANOVA test. Scale bar=30 μ M.

Figure 8. Macitentan impairs metastatic spread and inhibitsexpression of IQGAP1 and other invadopodia effectors.

(A) Female nude mice i.p. injected with SKOV3 cells (2×10^6) were treated after two weeks with vehicle control (CTR) or macitentan (MAC, 30 mg/kg) for 5 weeks. At the end of the treatment, all mice were euthanized and intraperitoneal organ were examined for visible metastasis. Value, mean \pm SD of eight mice from two independent experiments. Statistics were obtained using the one-way ANOVA test. Representative intraperitoneal nodules are indicated by white arrow heads. **(B)** Representative WB showing expression of IQGAP1, vinculin and MT1-MMP from metastatic nodules of xenografts treated as in A. Tubulin or β -actin was used for normalization. **(C)** Representative WB showing expression of phospho (p)-cortactin and cortactin from metastatic nodules of xenografts treated as in A. Tubulin was used for normalization. **(D)** Kaplan-Meier curves of progression-free survival (PFS) of ovarian cancer patients with low or high tumor expression of IQGAP1 or IQGAP1/ARRB1 or EDNRA/ARBB1/IQGAP1. **(E)** Proposed model of how ET-1/ β -arr1/IQGAP1 network affects invadopodia activity, ECM degradation and cell invasion. Activated ET-1R by ET-1 promotes the β -arr1/IQGAP1/RacGAP1 complex formation, leading to deactivation of Rac1 and activation of RhoA,C, which in turn promote invadopodia maturation and increased MMP secretion/activation with a consequent increase of cell invasion.

HIGHLIGHTS

- Endothelin-1 prompts IQGAP1/ β -arr1 to coordinate invasive invadopodia in serous ovarian cancer cells.
- Disrupting of IQGAP1/ β -arr1 interaction inhibits ET-1R-dependent invadopodia activation and cell invasion.
- In human patients, high expression of IQGAP1/ β -arr1/ ET_A R positively correlates with poor prognosis, suggesting this signature as new prognostic factor in ovarian cancer.
- Targeting of ET-1R inhibits SOC metastatic dissemination and invadopodia effectors expression, representing a novel therapeutic approach for serous ovarian cancer.

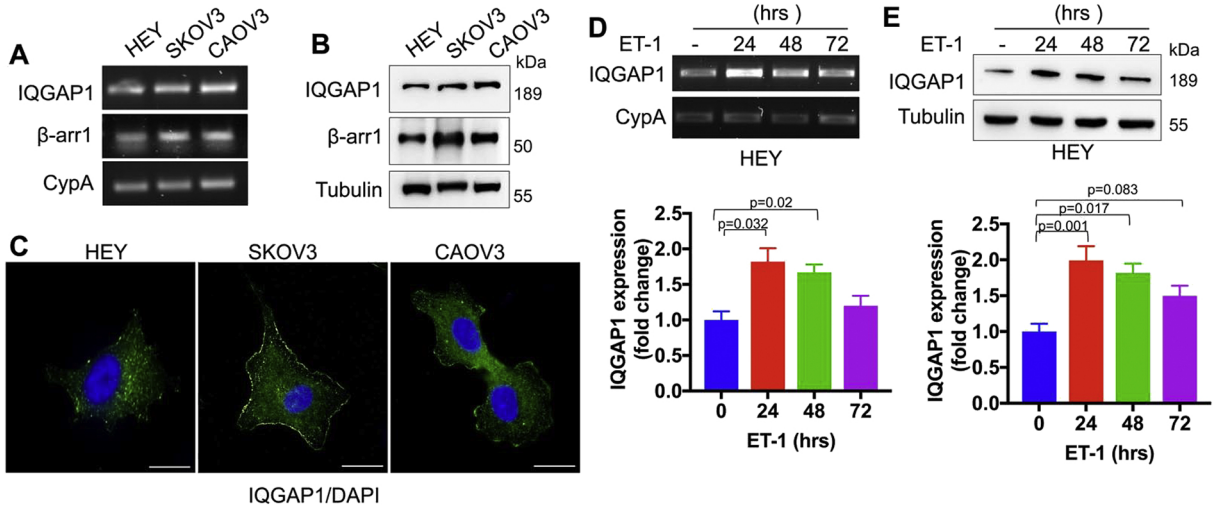


Figure 1

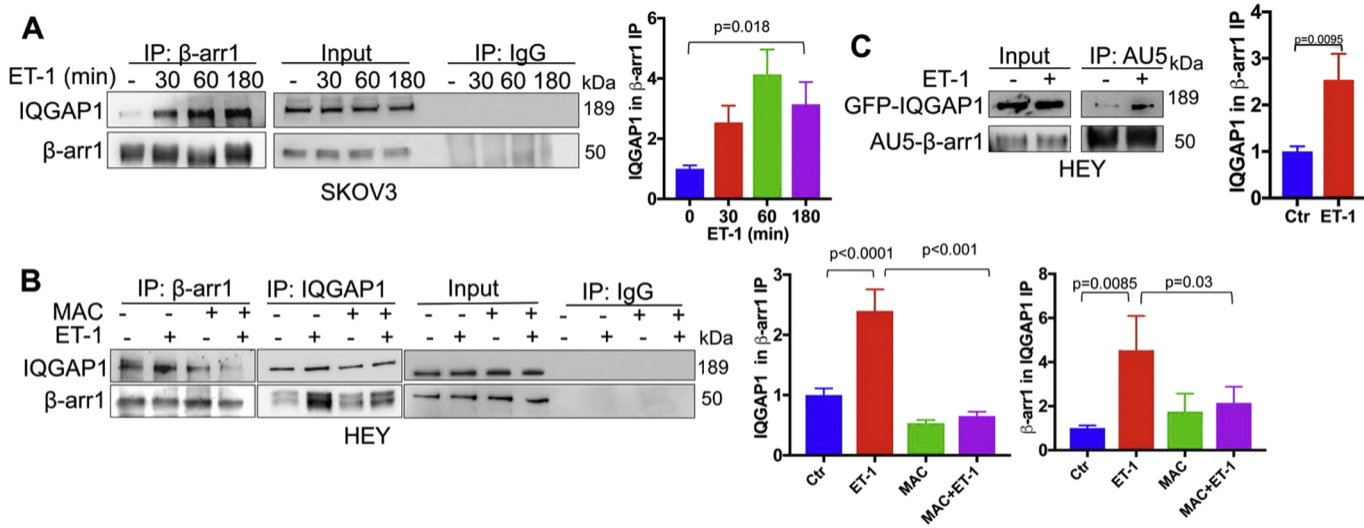


Figure 2

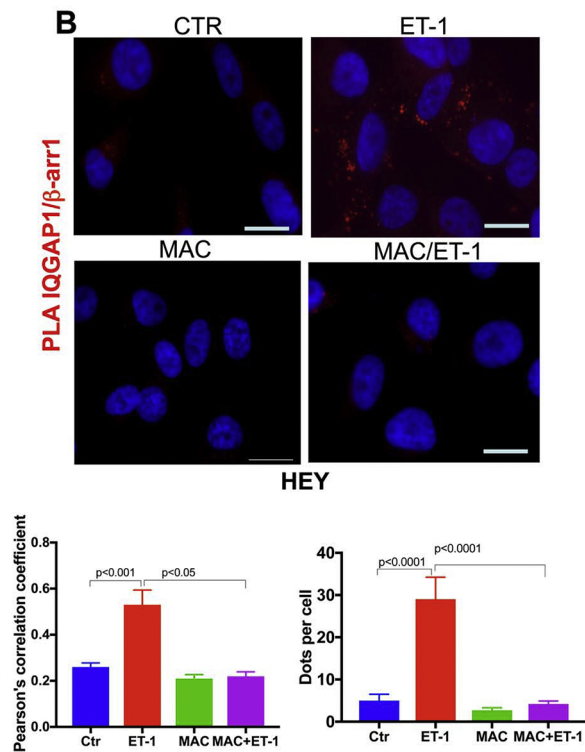
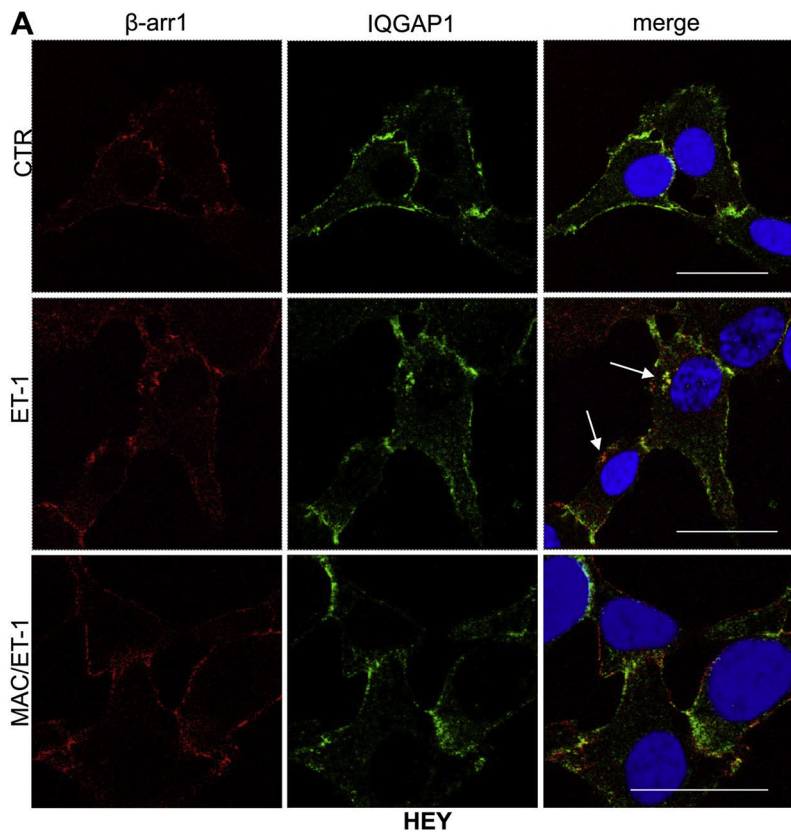


Figure 3

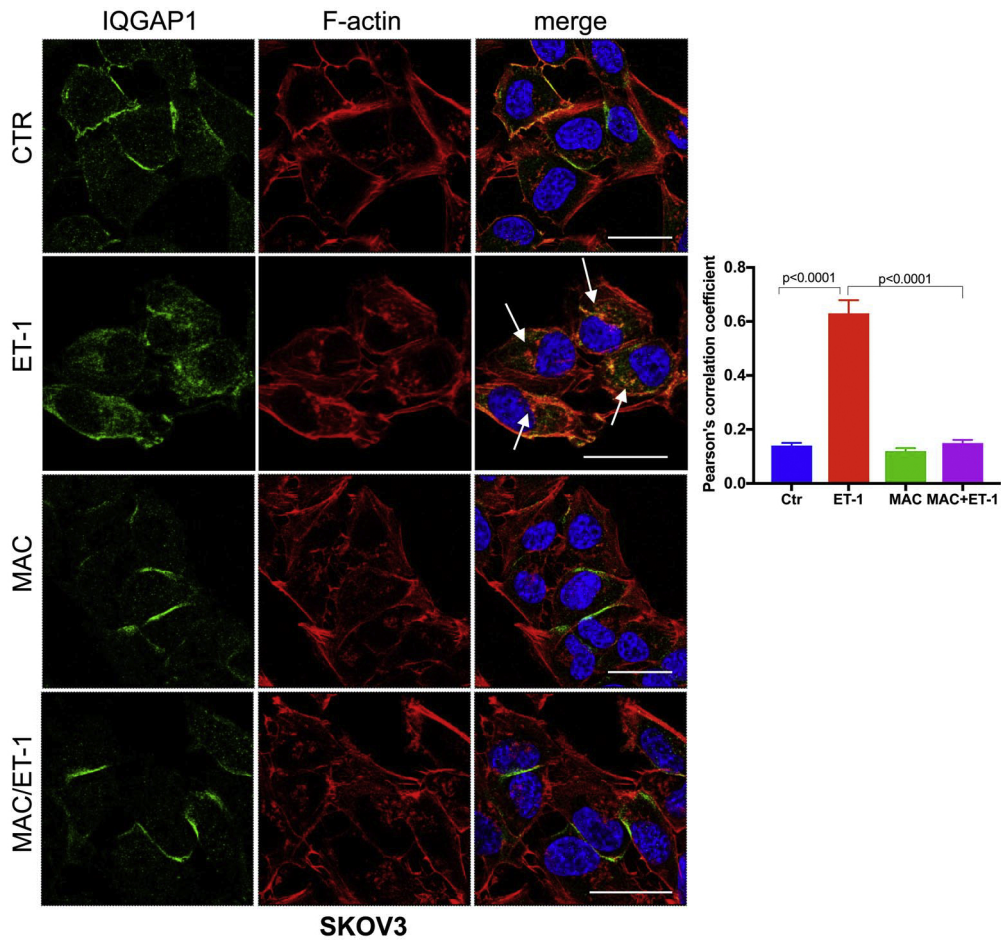
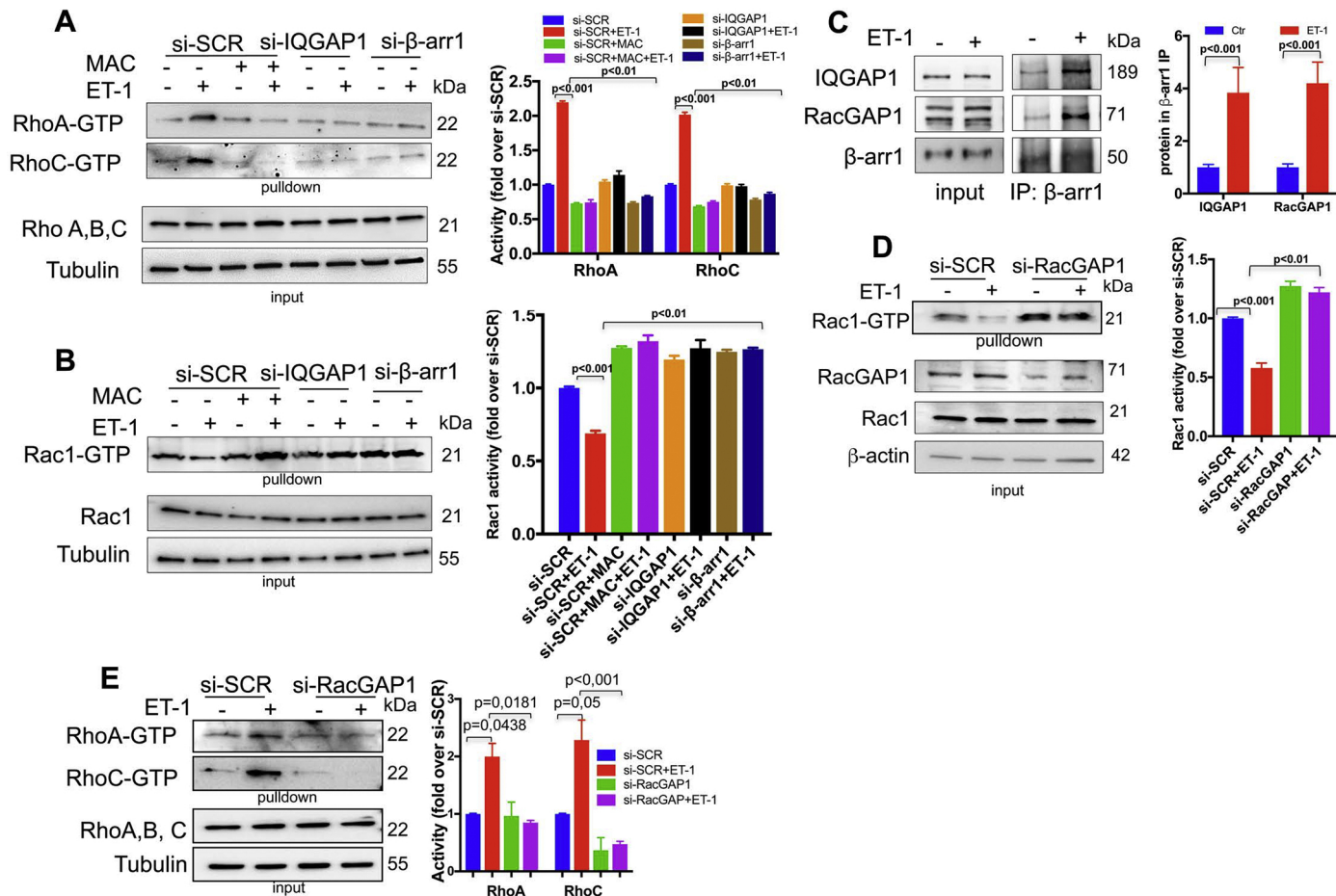


Figure 4



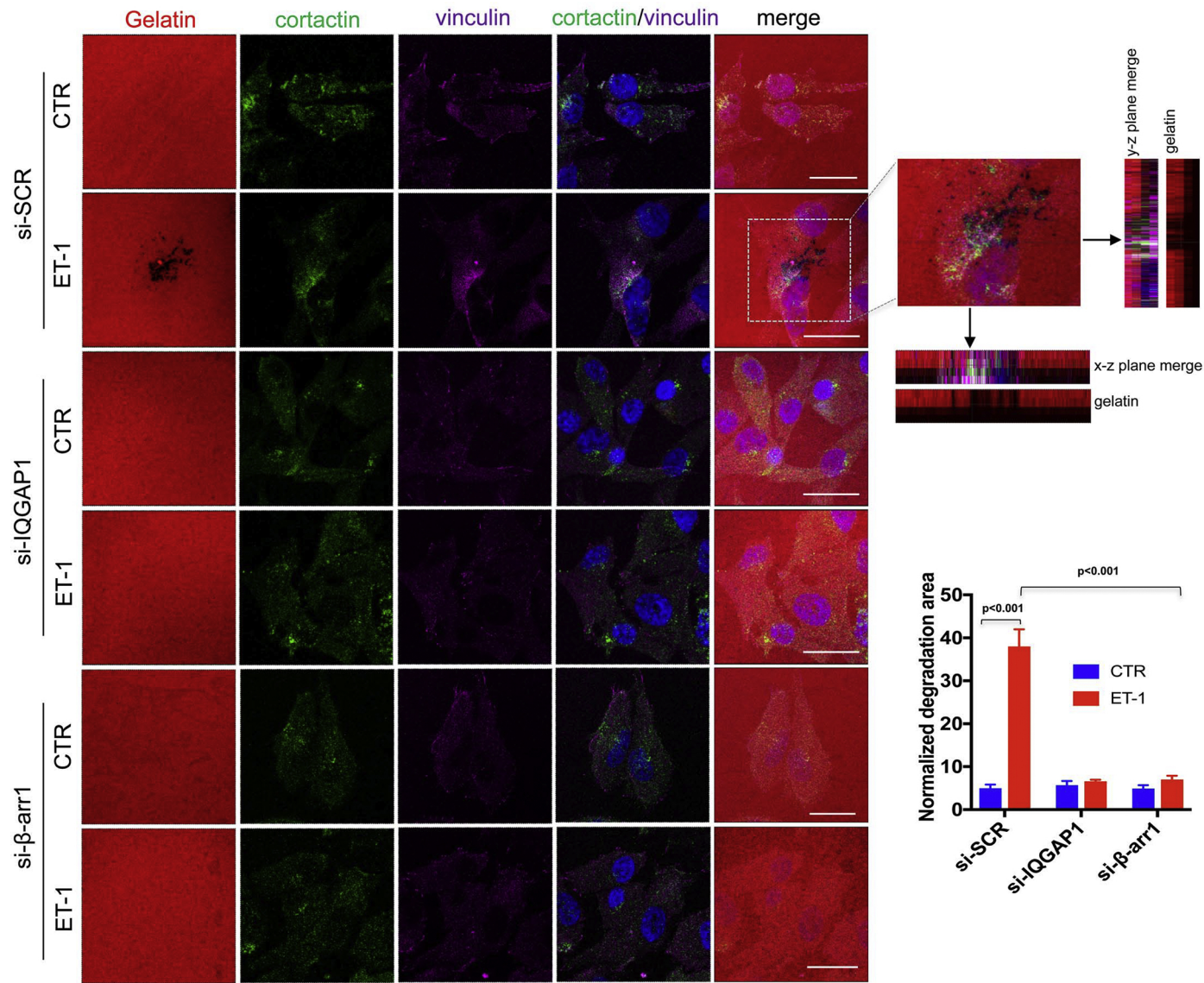


Figure 6

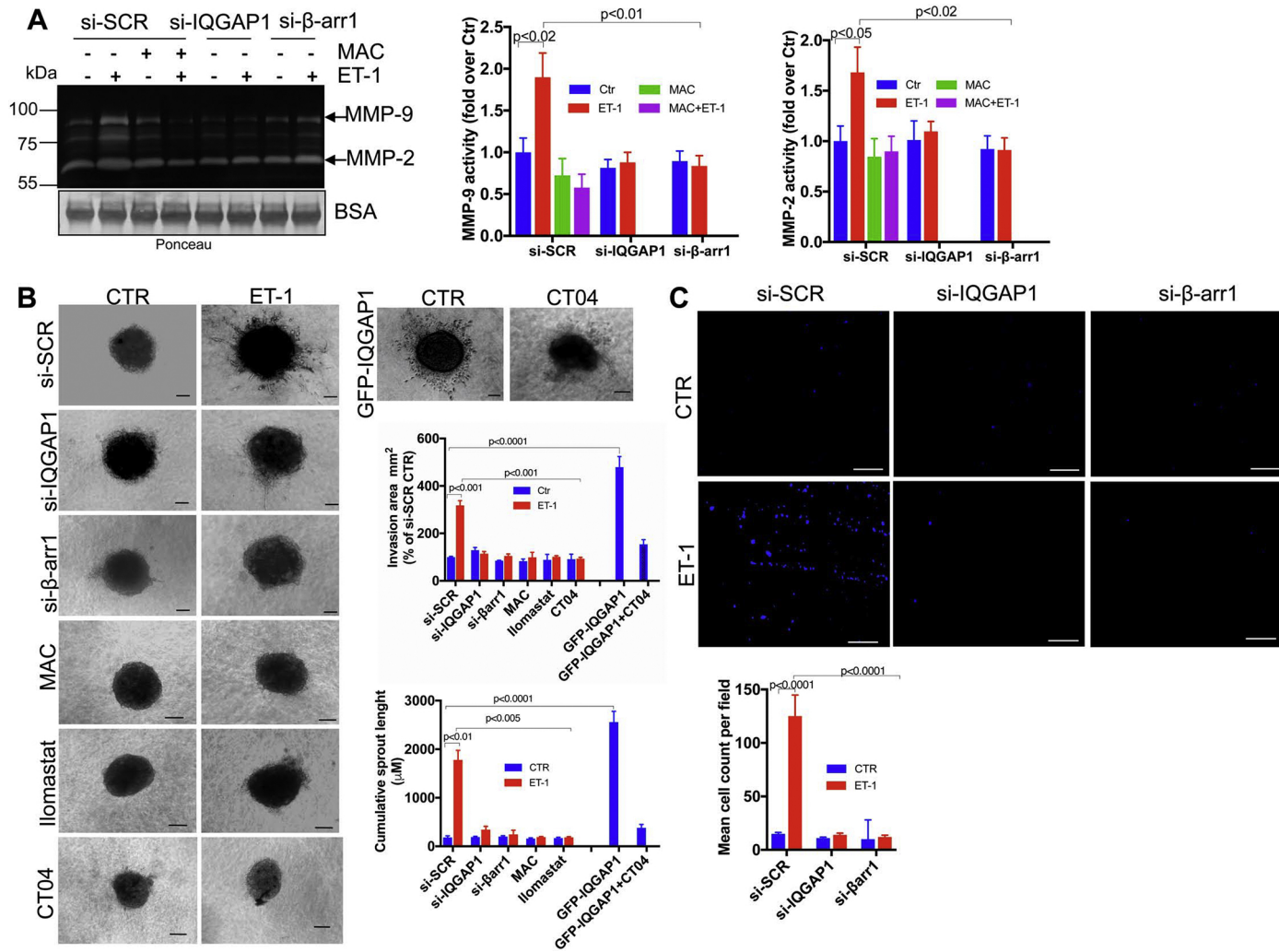


Figure 7

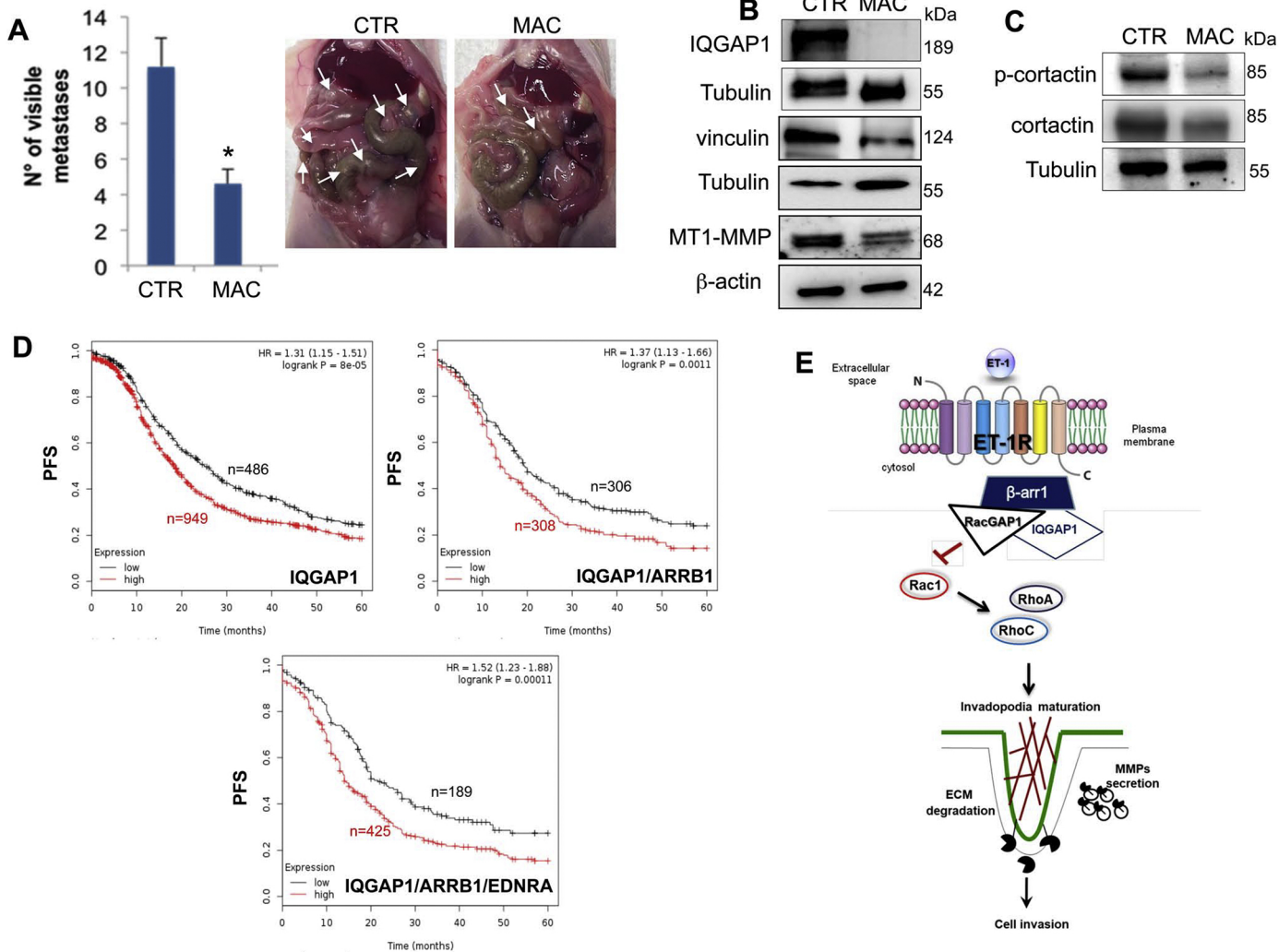


Figure 8